PAPER

Check for updates

Highly stable semitransparent solar cell employing graphene/WS₂/LaVO₃ vertical-heterostructure†

Da Hee Kim,‡[ab] Dong Hee Shin,‡[c] Dae Ho Jung,[ad] Si Duck Oh,[e] Eun Ji Kim[ab] and Hosun Lee 🆔 ★[abd]

Semi-transparent (ST) solar cells are attracting a lot of attention among researchers as they can effectively utilize solar energy in various fields such as building-integrated solar power generation and portable solar chargers. Here, we introduce an ST solar cell composed of triethylenetetramine (TETA)-doped graphene (Gr), WS_2, and $LaVO_3$. The device not only harvests solar energy thanks to its high light absorption in the ultraviolet-visible range but is also translucent due to its thin film composition. The photovoltaic parameters and average visible transmittance (AVT) of TETA-Gr/WS_2/$LaVO_3$ solar cells are highly dependent on the $LaVO_3$ film thickness (t). Considering the correlation between efficiency and visual effects, the device has power conversion efficiency (PCE) of 5.07% and 35% AVT at $t = 200$ nm, suggesting that it is suitable for ST solar cells. To maximize the translucent properties of the device, the PCE of the device was further improved to 5.64% by using an Al reflective mirror. The durability of the cell was confirmed to maintain 91 and 84% of the original PCE even under continuous illumination of 1 Sun at 60 °C temperature (T_a) and 30% relative humidity (RH) and 80 °C T_a/50% RH for 1000 h.

1. Introduction

Solar energy with its advantages of cleanliness, abundance, and accessibility, is emerging as one of the leading sources of renewable energy and one of the candidates to meet the future demand of the world.[1] For the continued growth of solar energy, the relatively low energy density of solar lighting must be addressed. An approach for increasing energy density is to manufacture semitransparent (ST) solar modules and integrate them into the undesirable transparent surfaces of skyscrapers and automobiles.[2] To prepare an effective ST solar cell, it is necessary to simultaneously satisfy optimized power conversion efficiency (PCE) and high average visible transmittance (AVT). Meanwhile, Si solar cells have high efficiency and excellent long-term stability, but their high reflectance requires additional processing and has limited visual effects, making

them unsuitable for translucent solar cells. From this point of view, organic- and perovskite-based solar cells have been spotlighted as the most promising candidates for ST solar cells.[3–12] Both solar cells have many advantages such as simple device fabrication at low cost, lightweight, and high efficiency, but their commercialization is still limited due to low durability in the atmosphere.[13–16]

Meanwhile, $LaVO_3$ film, one of the perovskite oxide materials, was introduced as an optimized material for the active layer of solar cells due to its high absorption coefficient in the ultraviolet (UV)-visible region.[17–19] $LaVO_3$ films with high absorption can be thinned and are suitable as active layers for translucent devices. Additionally, $LaVO_3$ materials are easy to supply and the price is economical.[20] Besides, the stability of $LaVO_3$-based optoelectronic devices has already been verified under atmospheric conditions as previously reported in the literature.[21–24] On the other hand, two-dimensional (2D) materials such as WS_2 are attracting much attention as optoelectronic devices owing to their strong light-material interactions useful for light absorption, noticeable band gaps, and high electron mobility.

Considering the advantages of 2D and $LaVO_3$ films, the 2D/$LaVO_3$ heterojunction structure is expected to provide better properties than single-component material-based optoelectronic devices.[24] Most recently, we successfully fabricated a chemical vapor deposition (CVD)-MoS_2/$LaVO_3$-based high-performance self-powered photodetector, demonstrating superior performance over other CVD-MoS_2-based devices.[24] Additionally, the same structural device showed photovoltaic properties under 1 sun

[a] *Department of Applied Physics, Kyung Hee University, Yongin 17104, Republic of Korea. E-mail: hlee@khu.ac.kr*

[b] *Education Institute for Frontier Science and Technology (BK21 Four), Kyung Hee University, Yongin 17104, Republic of Korea*

[c] *Department of Smart Sensors Engineering, Andong National University, Andong, Gyeongbuk, 36729, Republic of Korea*

[d] *Institute of Natural Sciences, Kyung Hee University, Yongin 17104, Republic of Korea*

[e] *Smart Energy and Nano Photonics R&D Group, Korea Institute of Industrial Technology (KITECH), Gwangju, 61012, Republic of Korea*

† Electronic supplementary information (ESI) available. See DOI: https://doi.org/10.1039/d3tc03411a

‡ These two authors have contributed equally to this study.

This journal is © The Royal Society of Chemistry 2024

J. Mater. Chem. C, 2024, **12**, 2843–2848 | **2843**

(100 mW cm^{-2}) illumination. In previous literature, we mentioned triethylenetetramine (TETA)- doped graphene (Gr) transparent conductive electrodes (TCEs).[25–27] TETA-Gr obtained excellent transmittance (T) at the wavelength of 300–1000 nm and low sheet resistance as well as n-type characteristics. Furthermore, TETA-Gr suggests long-term stability in the air and heat.[28] Considering the properties of each material, we selected a translucent active layer for WS$_2$ and LaVO$_3$ and a TCE for TETA-Gr. In other words, We fabricated TETA-Gr as a TCE for WS$_2$/LaVO$_3$ devices to maximize the properties of ST solar cells.

Here, WS$_2$ and LaVO$_3$ materials were elaborately selected to fabricate ST solar cells. In the TETA-Gr/WS$_2$/LaVO$_3$ heterojunction structure, efficient translucent solar cells were achieved by fine-tuning the thickness (t) of LaVO$_3$ from 70 to 300 nm. The PCE and AVT values of the ST cell can be tuned from 2.66 to 5.42% and from 55 to 26% as the LaVO$_3$ layer t increases from 70 to 300 nm. Furthermore, the efficiency was improved by 12% by adding an Al reflective mirror for the device with t = 200 nm. Finally, the durability of the device shows that the initial efficiency decreases by only 9 and 16% after 1000 h for 60 °C temperature (T_a) and 30% relative humidity (RH) and 80 °C T_a/50% RH under continuous air mass (AM) of 1.5 global (1 sun, 100 mW cm^{-2}), thereby indicating good stability.

2. Experimental section

2.1 Fabrication of graphene/WS$_2$/LaVO$_3$ semitransparent solar cells

To synthesize the LaVO$_3$ film on the quartz substrate, we used 50 W radio frequency sputtering equipment under an H$_2$ (35%)/Ar mixture gas atmosphere. Here, we varied the thickness of the LaVO$_3$ film by adjusting the sputtering time. Next, WS$_2$ was transferred onto the LaVO$_3$ film using a poly(methyl methacrylate) (PMMA) support film-based wet transfer method.[29] Here, the CVD-WS$_2$ sheet was purchased from Six Carbon Technology and is a uniformly grown sample on a SiO$_2$/Si substrate. PMMA-coated WS$_2$/SiO$_2$/Si samples were suspended in a buffered oxide etch bath to separate the SiO$_2$/Si substrate and washed several times in a deionized water bath. Sequentially, the CVD-monolayer Gr was transferred onto the WS$_2$ sheet by the same wet transfer process to finally fabricate the Gr/WS$_2$/LaVO$_3$ heterojunction structure. To prepare n-type Gr, a solution of TETA was dropped on the surface of Gr, followed by spin coating at 2500 rpm for 1 min. Then, the samples were dried at 75 °C for 10 min. TETA solutions were prepared by dissolving TETA molecules in ethanol. To finally complete the solar cell, Ag and Au films were used as the upper and lower electrodes, respectively. We fixed the active area of the devices to 20 × 20 mm^2.

2.2 Characterizations

The thicknesses of the LaVO$_3$ films were analyzed by field-emission scanning electron microscopy (FE-SEM) (Carl Zeiss, model LEO SUPRA 55). By atomic force microscopy (AFM, Park Systems), we checked the surface roughness of LaVO$_3$.

The Raman spectra of WS$_2$ and TETA-Gr were measured by a Raman spectroscopy system with a 532 nm laser. To confirm the uniform WS$_2$ sheet, we observed it through an optical microscope. The transmittance (T)/absorbance spectra of LaVO$_3$, WS$_2$, and TETA-Gr were analyzed by a UV-visible-near-infrared (NIR) spectrophotometer (Agilent Varian, model Carry 5000). The baseline was calibrated with a quartz substrate. With the 4-probe using van der Pauw method (Dasol Eng., model FPP-HS8-40K) and Kelvin probe force microscopy (KPFM) (Park systems, model XE100), we measured the sheet resistance and work function, respectively. To check the atomic bonding state of TETA-Gr, we measured and analyzed the spectrum by X-ray photoelectron spectroscopy (XPS) using an Al Kα line with 1486.6 eV. The photovoltaic parameters of the device were measured using a Keithley 2400 source meter under 1 Sun (100 mW cm^{-2}) illumination in the atmosphere. External quantum efficiency (EQE) was measured from wavelengths of 300–1000 nm from a system consisting of a monochromator and a light source and then calibrated from a commercial Si reference cell. To improve the efficiency of the device by reflecting light transmitted from the translucent solar cell, we used an Al reflective mirror.

3. Results and discussion

Fig. 1(a) presents real images of LaVO$_3$ films as a function of t. In Fig. 1(b), the average surface roughness (R_q) of 200 nm LaVO$_3$ is 0.421 nm, suggesting a relatively low roughness. From the cross-sectional FE-SEM image, it is indicated that 200 nm-LaVO$_3$ was grown uniformly, as shown in Fig. 1(c). Fig. 1(d) shows the XPS spectrum for LaVO$_3$ film at t = 200 nm. As shown in the XPS spectrum, the La 3d, V 2p, and O 1s core levels were observed, indicating that the LaVO$_3$ film was well synthesized. Fig. 1(e) and (f) shows the T/absorbance of LaVO$_3$/quartz for various t in the wavelength range of 300 to 1000 nm. With increasing t, the T spectrum gradually decreases while the absorbance spectrum gradually increases. In the T spectrum, the AVT corresponding to the wavelength of 400–800 nm decreases from 67 to 37% with increasing t from 70 to 300 nm.

We confirmed that the WS$_2$ sheets grew uniformly without pinholes by optical microscopy (Fig. S1a, ESI†). To confirm the t of the WS$_2$ film, we measured it to be about 3.8 nm by the line profile of the AFM topography image. (Fig. S1b, ESI†). In the XPS spectrum for WS$_2$, well-known peaks of W 4f$_{7/2}$, W 4f$_{5/2}$, W 5p$_{3/2}$, S 2p$_{3/2}$, and S 2p$_{1/2}$ were identified (Fig. S1c and d, ESI†). From the XPS spectrum, the atomic ratio of W and S was calculated to be 1:2, similar to the nominal stoichiometry of WS$_2$.[30] In the Raman spectrum for the WS$_2$ sheet, the representative E_{2g}^1 and A_{1g} peaks were identified (Fig. S1e, ESI†). To confirm the number of layers of the WS$_2$ sheet, we evaluated the difference between the peak positions of E_{2g}^1 and A_{1g}, thereby confirming that it was 4–5 layers,[31,32] consistent with the AFM results. To confirm the exact Fermi level of multilayer WS$_2$, we measured the work function using the KFPM and obtained 4.58 ± 0.03 eV (Fig. S1f, ESI†). The spectrum for the T
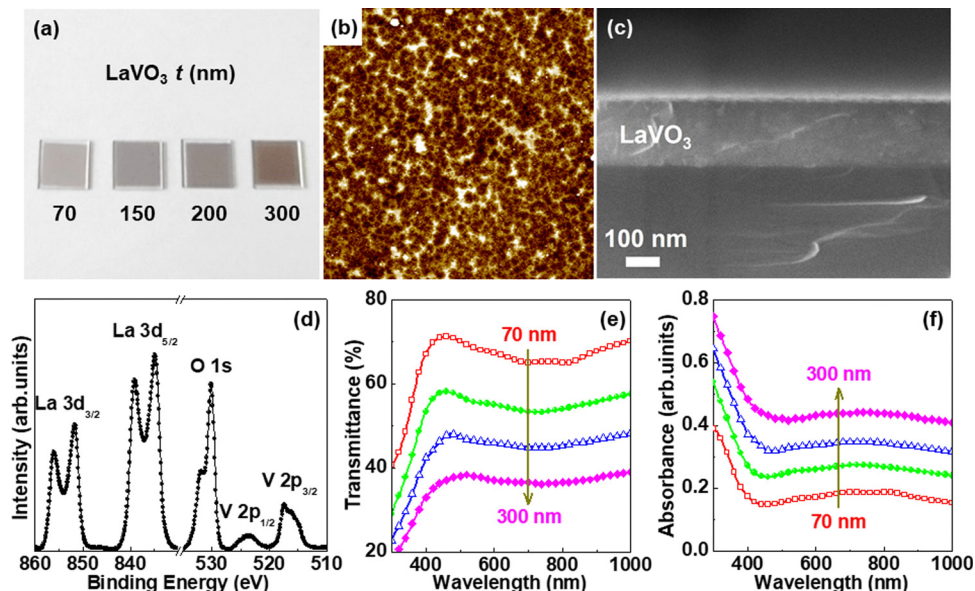
2844 | *J. Mater. Chem. C*, 2024, **12**, 2843–2848

This journal is © The Royal Society of Chemistry 2024

Fig. 1   (a) Real image of LaVO$_3$ film on quartz substrate as a function of t. (b) AFM topography image, (c) Cross-sectional SEM image, and (d) XPS spectrum of LaVO$_3$ film at t = 200 nm. (e) Transmittance and (f) Absorbance spectra of LaVO$_3$ film from wavelength of 300 to 1000 nm for various t.

and absorbance of the WS$_2$ film in the range of wavelength of 300 to 1000 nm is shown. (Fig. S1g, ESI†). As shown in the spectrum, T and absorbance show opposite trends. We suggest that WS$_2$ is a suitable material for translucent optoelectronic devices based on the appropriate absorbance and T in the visible light region.

Raman spectra show the G and 2D bands of pristine-Gr and TETA-Gr (Fig. S2a, ESI†). Both the G and 2D bands were blue-shifted by TETA doping, indicating charge transfer from the dopants to the Gr, thereby resulting in phonon softening.[28,33] To confirm whether the Gr surface was doped with the TETA dopant, we observed XPS spectra of the Gr sheet before and after doping (Fig. S2b, ESI†). As the N 1s peak is displayed only on the TETA-Gr surface, it is considered that the Gr surface is doped with the TETA dopant. To analyze the change in the work function of Gr by the TETA dopant, we measured the work function of pristine-Gr and TETA-Gr using the KPFM (Fig. S2c, ESI†). The work function of pristine-Gr is −4.57 eV, and after doping, it decreases to −4.41 eV, indicating n-type Gr characteristics. It was introduced that electron-donating aromatic molecules including -amine (–NH$_2$) and -dimethyl (–CH$_3$)

exhibit stable n-type properties in combination with Gr under atmospheric conditions, in previous literature.[28,33,34] The sheet resistances of Gr with and without TETA are 590 and 208 Ohm sq^{-1} (Fig. S2d, ESI†). In addition, the T of TETA-Gr shows no significant difference from that of pristine-Gr (Fig. S2e, ESI†). An optimized transparent conductive electrode should exhibit low sheet resistance and high T. These results suggest that TETA-Gr is an excellent TCE due to its high T and low sheet resistance.[35]

Fig. 2(a) shows a typical schematic and real image of the TETA-Gr/WS$_2$/LaVO$_3$ ST cells. The optical image shows that the regions of WS$_2$/LaVO$_3$ and TETA-Gr/WS$_2$/LaVO$_3$ are separated (Fig. S3a, ESI†). We specifically measured Raman spectra to distinguish between the two interfaces. The G and 2D Raman peaks of TETA-Gr were observed only in the Raman spectrum of TETA-Gr/WS$_2$/LaVO$_3$ (Fig. S3b, ESI†), consistent with the optical image. Fig. 2(b) shows the energy band diagram for the TETA-Gr/WS$_2$/LaVO$_3$ cell. Here, the Fermi energy (E_F) and conduction band/valence band (E_c/E_v) values were obtained from the measured results and previous literature.[21] When the sample is irradiated with 1 sun, free electrons and holes are generated in
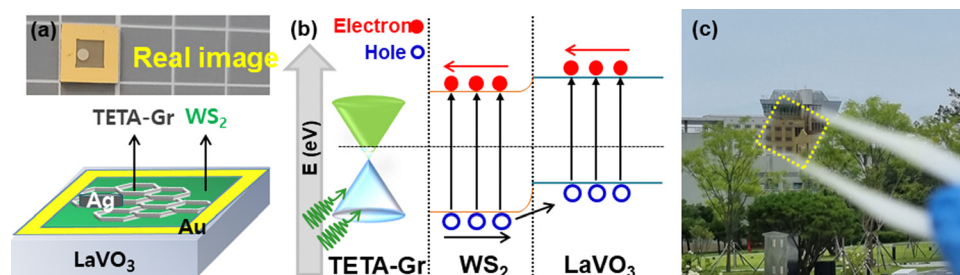

Fig. 2   (a) Real image/schematic device structure and (b) its energy band structure. (c) Photograph of a TETA–Gr/WS$_2$/LaVO$_3$ device (yellow dotted line). This photo shows the semitransparency of the device.

the WS_2 and $LaVO_3$ layers. The generated electrons and holes are transported/collected toward the TETA-Gr and Au electrodes. Fig. 2(c) shows that the building is visible through the device, suggesting a translucent solar cell.

Fig. 3(a) shows the current density–voltage (J–V) behavior of devices for various t under AM 1.5G illumination with an intensity of 100 mW cm^{-2}. From the J–V curve, we systematically analyzed the open-circuit voltage (V_{oc}), short-circuit current density (J_{sc}), fill factor (FF), and power conversion efficiency (PCE) of the t-dependent devices, as summarized in Table 1. As shown in Fig. 3(a) and Table 1, the V_{oc} of the device nearly remained unchanged from 0.45 V to 0.43 V with different t. Meanwhile, as t increases from 70 to 300 nm, $LaVO_3$ enhances light absorption, resulting in a gradual enhancement of J_{sc}. However, at $t \geq 200$ nm, J_{sc} does not increase significantly. As t increases, transfer resistance, charge accumulation, and transfer time improve, thereby reducing FF. However, the reduction of FF is largely offset by the increase in J_{sc}, resulting in higher efficiency for larger t. The ST solar cell exhibits the highest efficiency with 0.43 V V_{oc}, 20.20 mA cm^{-2} J_{sc}, 62.43% FF, and 5.42% PCE at t = 300 nm. As a control sample, pristine-Gr/WS_2/$LaVO_3$ cell displays efficiencies of 1.12–2.85% (Fig. S4a and Table S1, ESI†). The relatively low efficiency for pristine Gr-based ST cells is a result of the high sheet resistance of pristine Gr and the mismatch of the work function at the interface. Fig. 3(b) presents the external quantum efficiency (EQE) spectra from the wavelength of 300–1000 nm for t-dependent cells. As is well known, we calculated EQE from photo-harvesting efficiency, charge injection/transfer efficiency, and charge collection efficiency.[36] Consequently, the

Table 1 Photovoltaic parameters of the TETA-Gr/WS_2/$LaVO_3$ solar cells for various t

t (nm)	V_{oc} (V)	J_{sc} (mA cm^{-2})	FF (%)	PCE (%)	Integrated J_{sc} (mA cm^{-2})	AVT (%)
70	0.45	9.38	66.73	2.81	8.98	55
150	0.44	15.98	64.66	4.55	15.21	42
200	0.43	18.61	63.39	5.07	17.75	35
300	0.43	20.20	62.43	5.42	19.50	26

EQE of TETA-Gr-based cells gradually improved over almost the entire wavelength range as t increased from 70 to 300 nm (Fig. 3(b)). Likewise, devices with pristine-Gr showed the same trend (Fig. S4b, ESI†). The deviation between the integrated J_{sc} evaluated from the EQE spectrum and J_{sc} measured at 1 sun was within 5%, as summarized in Table 1. This feature is due to the close correlation between J_{sc} and integrated EQE values.[36,37]

Fig. 3(c) shows the T spectrum of TETA-Gr/WS_2/$LaVO_3$ cells as a function of t. As the t of $LaVO_3$ increases, the T for all wavelengths decreases due to the increase in light absorption. We evaluated the AVT associated with the wavelength of 400–800 nm range for all cells. As t increases from 70 to 300 nm, the AVT decreases from 55 to 26%, showing opposite trends. Fig. 3(d) plots the PCE *versus* AVT of the full cell. We observe clear trends such as: at the lowest 26% AVT, the PCE approaches 5.42% and decreases as the T increases. The efficiency of the most transparent cell with an AVT of 55% was about 2.81%. Considering the results of PCE and AVT, we believe that it is most suitable for ST solar cells at t = 200 nm. To maximize the benefits of the translucent solar cell properties, we measured the J–V behavior using an Al reflective mirror
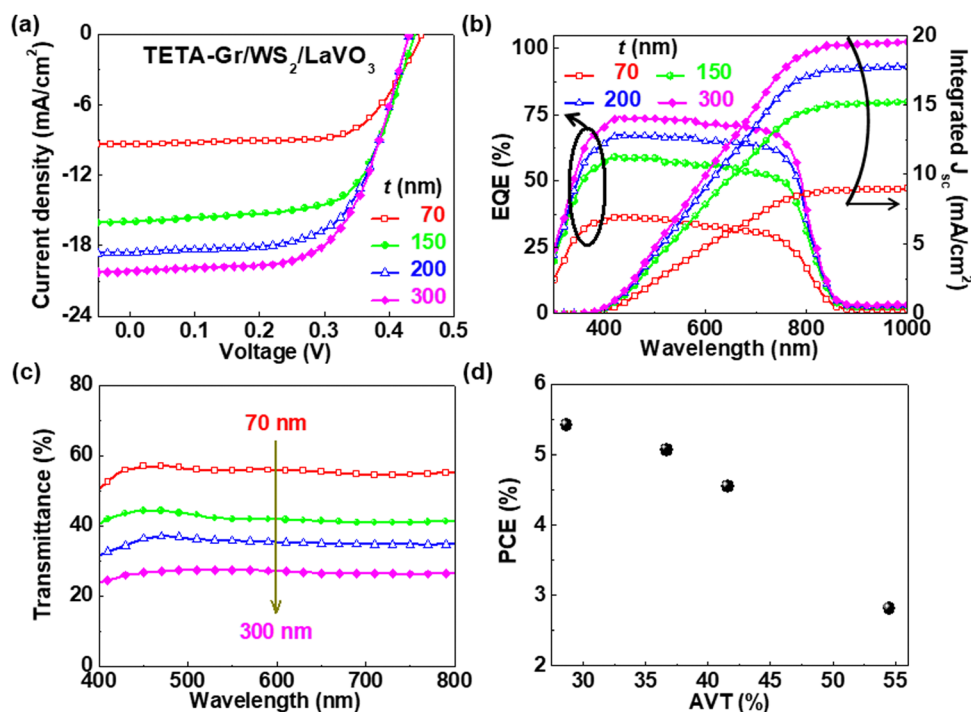

Fig. 3 (a) Photo J–V curves and (b) EQE spectra/integrated J_{sc} of TETA-Gr/WS_2/$LaVO_3$ solar cells for various t. (c) Spectral transmittance of a typical semitransparent solar cell on quartz. (d) Dependence of the average efficiency on the average visible transmittance of the device.
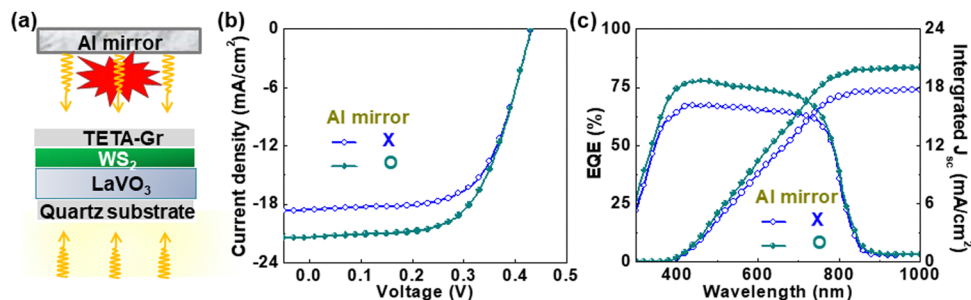
2846 | *J. Mater. Chem. C*, 2024, **12**, 2843–2848

This journal is © The Royal Society of Chemistry 2024

Fig. 4 (a) Schematic diagram illustrating the measurement method of a semitransparent solar cell equipped with an Al reflective mirror. (b) J–V curves of the semitransparent cell for t = 200 nm without/with an Al reflective mirror. (c) EQE spectra of devices without/with Al mirror.

for t = 200 nm. Here, the Al mirror helps re-absorption of the device by reflecting the light in the UV-visible region, as shown in the schematic diagram of Fig. 4(a). In the system with Al mirrors, the efficiency of the device was 5.64%, an improvement of approximately 12% compared to the device without mirrors, as summarized in Table 2 (Fig. 4(b)).

Fig. 4(c) shows the EQE spectra of devices with/without Al mirrors. The integrated J_{sc} of both devices is 18.61 and 21.40 mA cm^{-2}, respectively, suggesting improved EQE over a wide wavelength range of 350–800 nm compared to Al mirror-free based devices. This demonstrates a significant improvement in J_{sc} due to the increased light harvesting efficiency thanks to the Al mirror.

Finally, we measured the J–V properties under continuous 1 sun with 60 °C temperature (T_a)/30% relative-humidity (RH) and 80 °C T_a/50% RH to check the stability of the device including 5.02% PCE and 35% AVT. Fig. 5(a) shows the evolution of PCE during 1000 h under 1 sun. Fig. 5(b) and (c) shows the J–V curves of the device before and after continuous 1-sun illumination for two conditions. As a result, the devices changed slightly from 5.01% to 4.51 and 4.23% for 60 °C T_a/30% RH and 80 °C T_a/50% RH, respectively, maintaining 91 and 84% of the original PCE. The stability of TETA-Gr TCE was also monitored for sheet resistance under the same conditions (60 °C T_a/30% RH and 80 °C T_a/50% RH). The initial sheet resistance of TETA-Gr TCE before illumination was 208 ± 12 Ohm sq^{-1}. After 1000 h, the sheet resistance increased by ~1.07/1.15 times the initial value for 60 °C T_a/30% RH and 80 °C T_a/50% RH, respectively (Fig. S5, ESI†). This confirmed that cell deterioration can be mainly caused by an increase in sheet resistance of TETA-Gr, but the increase in sheet resistance is not significant, resulting in a small decrease in efficiency. It is believed that the source of this high stability comes from the excellent chemical and thermal stability of TETA-Gr, WS$_2$, and LaVO$_3$ materials, as reported in previous literature.[21,28,38–40] These

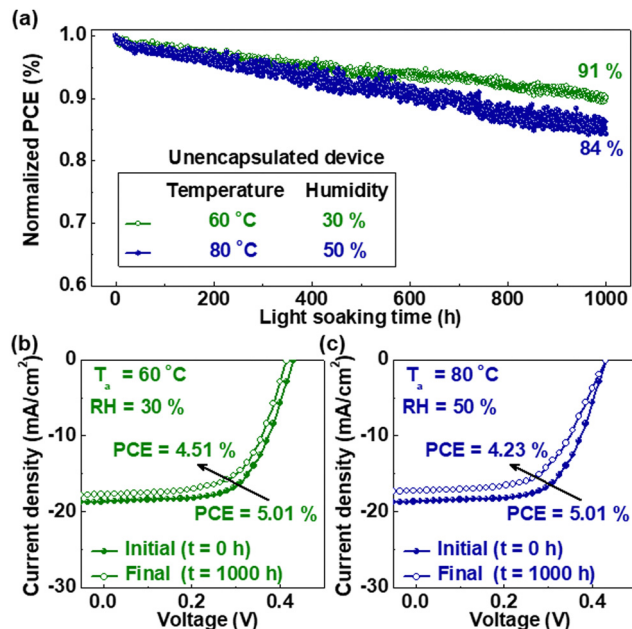**Fig. 5** (a) Photo-stabilities of TETA-Gr/WS$_2$/LaVO$_3$ solar cells under continuous illumination of 1 Sun for 1000 h at 60 °C temperature (T_a)/30% relative-humidity (RH) and 80 °C T_a/50% RH. J–V curves of the solar cells for initial (t = 0 h) and final (t = 1000 h) under (b) 60 °C T_a/30% RH and (c) 80 °C T_a/50% RH.

results demonstrate that TETA-Gr/WS$_2$/LaVO$_3$ ST solar cells are excellent in photo-stability.

4. Conclusion

We have successfully demonstrated a novel ST solar cell using a translucent and photoactive LaVO$_3$ layer and TETA-Gr TCE. With increasing t, the efficiency of the device increased from 2.66 to 5.42%, but the AVT decreased from 55 to 26%. A good ST solar cells must meet high efficiency and visual effects. Considering efficiency and AVT, translucent solar cells are considered to have the optimal condition at t = 200 nm. The PCE of the ST solar cell was improved by approximately 12% by adding an Al reflective mirror compared to a system without an Al mirror. Furthermore, the PCE of the TETA-Gr/WS$_2$/LaVO$_3$ device decreased by only 9 and 16% compared to the initial PCE

Table 2 Photovoltaic parameters of the semitransparent solar cells without/with Al mirror

Light reflection	V_{oc} (V)	J_{sc} (mA cm^{-2})	FF (%)	PCE (%)
No mirror	0.43	18.61	63.39	5.07
With mirror	0.43	21.40	61.03	5.64

This journal is © The Royal Society of Chemistry 2024

J. Mater. Chem. C, 2024, **12**, 2843–2848 | **2847**

even after 1000 h under 1 sun in an atmosphere of 60 $^{\circ}$C T_a/30% RH and 80 $^{\circ}$C T_a/50% RH, respectively, demonstrating thermal stability.

Conflicts of interest

There are no conflicts to declare.

Acknowledgements

References

1 M. H. Alsharif, J. Kim and J. H. Kim, *Sustainability*, 2018, **10**, 1822.

2 S. Kim, M. Patel, S.-M. Youn, Y. Kim, K. Lee and J. Kim, *Mater. Today Energy*, 2023, **31**, 101203.

3 S.-H. Lim, H.-J. Seok, M.-J. Kwak, D.-H. Choi, S.-K. Kim, D.-H. Kim and H.-K. Kim, *Nano Energy*, 2021, **82**, 105703.

4 S. Yoon, H. U. Ha, H.-J. Seok, H.-K. Kim and D.-W. Kang, *Adv. Funct. Mater.*, 2022, **32**, 2111760.

5 S. Lie, A. Bruno, L. H. Wong and L. Etgar, *ACS Appl. Mater. Interfaces*, 2022, **14**, 11339–11349.

6 Y.-W. Zhang, P.-P. Cheng, W.-Y. Tan and Y. Min, *Appl. Surf. Sci.*, 2021, **537**, 147908.

7 G. Giuliano, A. Bonasera, G. Arrabito and B. Pignataro, *Sol. RRL*, 2021, **5**, 2100702.

8 D. Wang, H. Liu, Y. Li, G. Zhou, L. Zhan, H. Zhu, X. Lu, H. Chen and C.-Z. Li, *Joule*, 2021, **5**, 945–957.

9 G. P. Kini, S. J. Jeon and D. K. Moon, *Adv. Funct. Mater.*, 2021, **31**, 2007931.

10 X. Huang, L. Zhang, Y. Cheng, J. Oh, C. Li, B. Huang, L. Zhao, J. Deng, Y. Zhang, Z. Liu, F. Wu, X. Hu, C. Yang, L. Chen and Y. Chen, *Adv. Funct. Mater.*, 2022, **32**, 2108634.

11 J. Jing, S. Dong, K. Zhang, Z. Zhou, Q. Xue, Y. Song, Z. Du, M. Ren and F. Huang, *Adv. Energy Mater.*, 2022, **12**, 2200453.

12 Z. Hu, J. Wang, X. Ma, J. Gao, C. Xu, X. Wang, X. Zhang, Z. Wang and F. Zhang, *J. Mater. Chem. A*, 2021, **9**, 6797–6804.

13 T. A. Chowdhury, M. A. B. Zafar, M. S.-U. Islam, M. Shahinuzzaman, M. A. Islam and M. U. Khandaker, *RSC Adv.*, 2023, **13**, 1787–1810.

14 H. H. Park, *Nanomaterials*, 2022, **12**, 112.

15 L. A. Frolova, Q. Chang, S. Y. Luchkin, D. Zhao, A. F. Akbulatov, N. N. Dremova, A. V. Ivanov, E. E. M. Chia, K. J. Stevenson and P. A. Troshin, *J. Mater. Chem. C*, 2019, **7**, 5314–5323.

16 P. Jiang, L. Hu, L. Sun, Z. Li, H. Han and Y. Zhou, *Chem. Sci.*, 2022, **13**, 4714–4739.

17 H. T. Zhang, M. Brahlek, X. Ji, S. Lei, J. Lapano, J. W. Freeland, V. Gopalan and R. Engel-Herbert, *ACS Appl. Mater. Interfaces*, 2017, **9**, 12556–12562.

18 L. Wang, Y. Li, A. Bera, C. Ma, F. Jin, K. Yuan, W. Yin, A. David, W. Chen, W. Wu, W. Prellier, S. Wei and T. Wu, *Phys. Rev. Appl.*, 2015, **3**, 064015.

19 M. Jellitea, J.-L. Rehspringerb, M. A. Fazioc, D. Mullera, G. Schmerberb, G. Ferblantiera, S. Colisb, A. Diniab, M. Sugiyamad, A. Slaouia, D. Cavalcolic and T. Fix, *Sol. Energy*, 2018, **162**, 1–7.

20 C. Sun, J. A. Alonso and J. Bian, *Adv. Energy Mater.*, 2020, **11**, 2000459.

21 D. H. Jung, J. W. Hwang, J. J. Lee, D. H. Shin and H. Lee, *J. Alloys Compd.*, 2022, **904**, 163818.

22 J. J. Lee, D. H. Jung, D. H. Shin and H. Lee, *Nanotechnology*, 2022, **33**, 395202.

23 D. H. Shin, D. H. Jung and H. Lee, *ACS Omega*, 2023, **8**, 18695–18701.

24 J. J. Lee, D. H. Shin, D. H. Jung, S. D. Oh and H. Lee, *J. Alloys Compd.*, 2023, **937**, 168404.

25 D. H. Shin, J. S. Ko, S. K. Kang and S.-H. Choi, *ACS Appl. Mater. Interfaces*, 2020, **12**, 4586–4593.

26 J. M. Kim, S. Kim and S.-H. Choi, *ACS Sustainable Chem. Eng.*, 2019, **7**, 734–739.

27 D. H. Shin, C. W. Jang, H. S. Lee, S. W. Seo, S. Kim and S.-H. Choi, *Appl. Surf. Sci.*, 2018, **433**, 181–187.

28 I. Jo, Y. Kim, J. Moon, S. Park, J. S. Moon, W. B. Park, J. S. Lee and B. H. Hong, *Phys. Chem. Chem. Phys.*, 2015, **17**, 29492–29495.

29 A. J. Watson, W. Lu, M. H. D. Guimãraes and M. Stöhr, *2D Mater.*, 2021, **8**, 032001.

30 S. Riccardo, M. Elisabetta, A. Davide, N. Concetta, M. Rosanna, R. Simona, G. Cinzia, D. C. Pantaleo, R. Aurora and M. Cosimino, *Nanomaterials*, 2021, **11**, 1969.

31 Y. Li, X. Li, T. Yu, G. Yang, H. Chen, C. Zhang, Q. Feng, J. Ma, W. Liu, H. Xu, Y. Liu and X. Liu, *Nanotechnology*, 2018, **29**, 124001.

32 W. Zhao, Z. Ghorannevis, K. K. Amara, J. R. Pang, M. Toh, X. Zhang, C. Kloc, P. H. Tane and G. Eda, *Nanoscale*, 2013, **5**, 9677–9683.

33 Y. Kim, J. Ryu, M. Park, E. S. Kim, J. M. Yoo, J. Park, J. H. Kang and B. H. Hong, *ACS Nano*, 2014, **8**, 868–874.

34 X. Dong, D. Fu, W. Fang, Y. Shi, P. Chen and L.-J. Li, *Small*, 2009, **5**, 1422–1426.

35 S. De and J. N. Coleman, *ACS Nano*, 2010, **4**, 2713–2720.

36 J. D. Servaites, M. A. Ratner and T. J. Marks, *Appl. Phys. Lett.*, 2009, **95**, 163302.

37 M. Saliba, E. Unger, L. Etgar, J. Luo and T. J. Jacobsson, *Nat. Commun.*, 2023, **14**, 5445.

38 Y. Liua, W. Huang, W. Chen, X. Wang, J. Guo, H. Tian, H. Zhang, Y. Wang, B. Yu, T.-L. Ren and J. Xu, *Appl. Surf. Sci.*, 2019, **481**, 1127–1132.

39 J. D. Yao, Z. Q. Zheng, J. M. Shao and G. W. Yang, *Nanoscale*, 2015, **7**, 14974–14981.

40 S. Pace, M. Ferrera, D. Convertino, G. Piccinini, M. Magnozzi, N. Mishra, S. Forti1, F. Bisio, M. Canepa, F. Fabbri and C. Coletti, *J. Phys. Mater.*, 2021, **4**, 024002.

2848 | *J. Mater. Chem. C*, 2024, **12**, 2843–2848

This journal is © The Royal Society of Chemistry 2024